




The Sausage Globular Clusters

G. C. Myeong¹ , N. W. Evans¹, V. Belokurov¹, J. L. Sanders¹, and S. E. Koposov^{1,2} ¹Institute of Astronomy, University of Cambridge, Madingley Road, Cambridge CB3 0HA, UK²McWilliams Center for Cosmology, Department of Physics, Carnegie Mellon University, 5000 Forbes Avenue, Pittsburgh, PA 15213, USA

Received 2018 May 7; revised 2018 July 27; accepted 2018 August 2; published 2018 August 17

Abstract

The *Gaia* Sausage is an elongated structure in velocity space discovered by Belokurov et al. using the kinematics of metal-rich halo stars. They showed that it could be created by a massive dwarf galaxy ($\sim 5 \times 10^{10} M_{\odot}$) on a strongly radial orbit that merged with the Milky Way at a redshift $z \lesssim 3$. This merger would also have brought in globular clusters (GCs). We seek evidence for the associated Sausage Globular Clusters (GCs) by analyzing the structure of 91 Milky Way GCs in action space using the *Gaia* Data Release 2 catalog, complemented with *Hubble Space Telescope* proper motions. There is a characteristic energy E_{crit} that separates the in situ objects, such as the bulge/disk clusters, from the accreted objects, such as the young halo clusters. There are 15 old halo GCs that have $E > E_{\text{crit}}$. Eight of the high-energy, old halo GCs are strongly clumped in azimuthal and vertical action, yet strung out like beads on a chain at extreme radial action. They are very radially anisotropic ($\beta \sim 0.95$) and move on orbits that are all highly eccentric ($e \gtrsim 0.80$). They also form a track in the age–metallicity plane compatible with a dwarf galaxy origin. These properties are consistent with GCs associated with the merger event that gave rise to the *Gaia* Sausage.

Key words: galaxies: kinematics and dynamics – galaxies: structure

1. Introduction

There are multiple and striking pieces of evidence for the existence of a massive ancient merger that provides the bulk of the stars in the inner halo of the Milky Way galaxy. For example, the radial density profile of the stellar halo shows a dramatic break at around 30 kpc in tracers such as RR Lyrae and blue horizontal branch stars (e.g., Watkins et al. 2009; Deason et al. 2011). Deason et al. (2013) argued that this could be interpreted as the last apocenter of a massive progenitor galaxy accreted between 8 and 10 Gyr ago. Myeong et al. (2018a) showed that the kinematics of metal-rich halo stars ($-1.9 < [\text{Fe}/\text{H}] < -1.1$) betray extensive evidence of recent accretion using the Sloan Digital Sky Survey (SDSS)-*Gaia* catalog. The variation in Oosterhoff classes of RR Lyraes with radius (Belokurov et al. 2018a) similarly shows evidence that the bulk of the field RRab is provided by a single massive progenitor. Finally, Belokurov et al. (2018b) demonstrated that the shape of the velocity ellipsoid of the inner metal-rich stellar halo is highly non-Gaussian and sausage-shaped. They interpreted this *Gaia* Sausage as evidence that two-thirds of the local stellar halo could have been deposited via the disruption of a massive ($\gtrsim 10^{10} M_{\odot}$) galaxy on a strongly radial orbit between redshift $z = 3$ and $z = 1$. Although identified in the SDSS-*Gaia* catalog, recent investigations by Haywood et al. (2018) with the new *Gaia* Data Release 2 (DR2) catalog (Gaia Collaboration et al. 2018) support the original hypothesis. If so, then this beast must have brought with it a population of globular clusters (GCs), now dispersed in the inner halo. After all, the similarly massive Sagittarius galaxy (Sgr) is now known to have brought at least four and possibly seven GCs with it (e.g., Forbes & Bridges 2010; Sohn et al. 2018).

The main aim of this Letter is to search for the Sausage Globular Clusters. The identification of objects accreted in the same merger event is easiest in action space. Actions have the property of adiabatic invariance, so that they stay

approximately constant when changes in the potential occur slowly (e.g., Goldstein 1980; Binney & Spergel 1982). GCs accreted in the same event are identifiable as clumped and compact substructures in action space (as is indeed the case for the 4 Sgr GCs—Terzan 7, Terzan 8, Arp 2, and Pal 12). Historically, actions were cumbersome to calculate, but recent theoretical advances have transformed the situation (e.g., Binney 2012; Sanders & Binney 2016). The power of actions has recently been demonstrated by the identification of the tidal disorgements of ω Centauri (Myeong et al. 2018b). Here, we display the Milky Way GCs in action space using a realistic Galactic potential comprising flattened stellar and gas disks, halo, and bulge (McMillan 2017) with the specific aim of identifying the Sausage GCs.

2. The GCs in Action Space

The Milky Way GCs are a disparate group: some were formed in situ in the Milky Way, some were acquired by the engulfment of dwarf galaxies. A classification was introduced by Zinn (1993), in which GCs are divided into bulge/disk, old halo, and young halo on the basis of cluster metallicity and horizontal branch morphology. The bulge/disk (BD) systems are concentrated in the Galactic bulge and inner disk, while the old halo (OH) clusters are predominantly in the inner halo. They are mostly believed to have been formed in the Milky Way, though $\sim 15\%$ – 17% might have been accreted. The young halo (YH) clusters can extend to large radii and are all believed to have been accreted (see e.g., Mackey & Gilmore 2004; Mackey & van den Bergh 2005).

The combination of observables from the Gaia Collaboration et al. (2018), Sohn et al. (2018), and Harris (1996, 2010 edition) allows us to obtain full six-dimensional information for 91 GCs (out of a total of ~ 150 in the Galaxy). To convert from observables to the Galactic rest-frame, we use the circular speed of 232.8 km s^{-1} at the Sun's position of 8.2 kpc, consistent with the McMillan (2017) potential, while for the

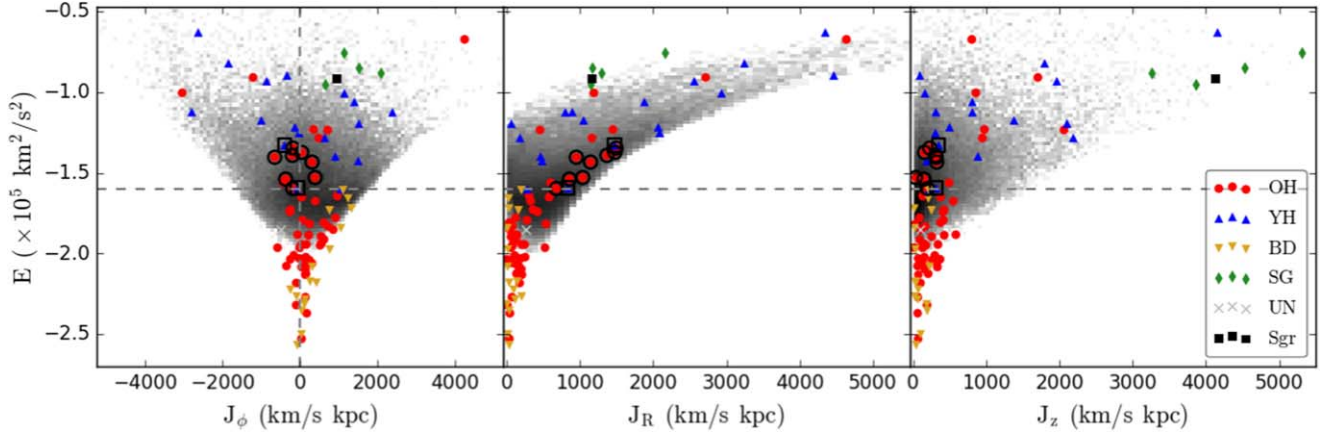


Figure 1. Distribution of GCs in energy-action space or (J_ϕ, E) , (J_R, E) , and (J_z, E) space. The grayscale background shows the halo MSTO stars from Myeong et al. (2018a) as a comparison. There are 75 GCs with *Gaia* DR2 proper motions and a further 16 with *Hubble Space Telescope* (*HST*) proper motions; 53 OHs (red circles), 17 YHs (blue triangles), 16 BDs (yellow triangles), and 4 Sgr GCs (SG; green diamonds) together with one of unknown classification (gray cross). Sgr is also marked as a black filled square. The vertical dashed line marks the division between prograde ($J_\phi > 0$) and retrograde ($J_\phi < 0$). The horizontal dashed line signifies the characteristic energy above which all of the YHs lie, and below which all of the BDs lie. The eight OH globular clusters, with symbols that are enclosed by black open circles, are grouped together in (J_ϕ, E) and (J_z, E) , while in (J_R, E) they are stretched out close to the boundary of J_R at corresponding energy (as judged from the MSTOs). They are the Sausage GCs. The two YHs enclosed with black open squares form an extended selection that may also be related. They have horizontal branch morphology similar to OHs, and have similar actions.

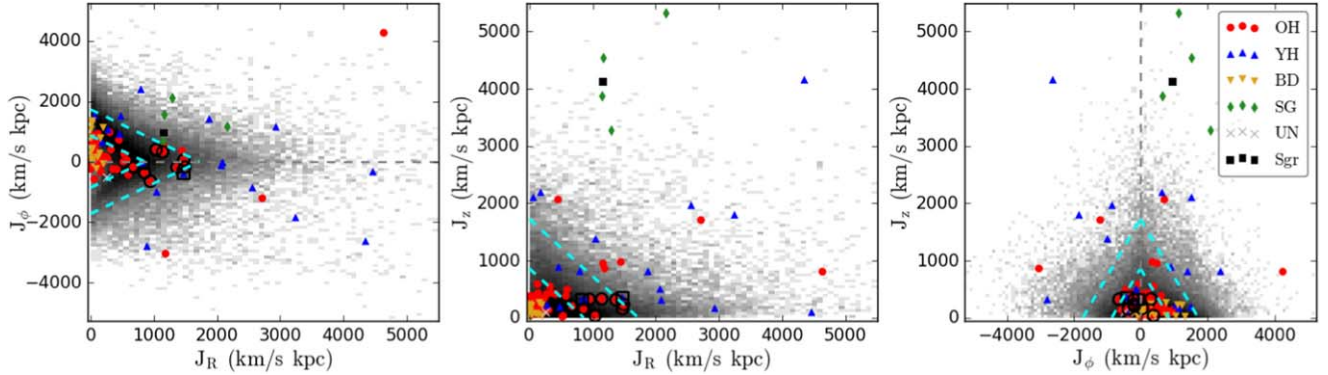


Figure 2. The same data as Figure 1, but now in action space. The Sausage GCs form an extended sequence in J_R , but are tightly clustered in J_ϕ and especially J_z . Again, black circles enclose probable members, black open squares possibles; red circles are OHs, blue triangles are YHs, yellow triangles are BDs, green diamonds are SGs, and the gray cross is unknown. The black filled square is Sgr itself. The gray dashed line marks $J_\phi = 0$. The two cyan dashed lines mark two constant-energy surfaces projected onto the principal planes to provide a rough idea of the action space morphology (see e.g., Figure 3.25 of Binney & Tremaine 2008).

Solar peculiar motion we use the most recent value from Schönrich et al. (2010), namely $(U, V, W) = (11.1, 12.24, 7.25) \text{ km s}^{-1}$. These values differ from those used by the *Gaia* Collaboration et al. (2018) or Posti & Helmi (2018), so there are small differences in quantities such as apocenters and eccentricities. We use the numerical method of Binney (2012) and Sanders & Binney (2016) to compute the action variables of each GC (J_R, J_ϕ, J_z). GCs associated with the *Gaia* Sausage must lie on highly radial orbits, and so have low J_ϕ and J_z , but very large J_R . The uncertainty in proper motions is the main contributor to the median (total) velocity error of $\sim 9 \text{ km s}^{-1}$. This leads to median errors in the actions of $\sim 10\%$, and so features in action space are robust against uncertainties. Figure 1 presents the distribution of GCs in energy and action space, while Figure 2 presents the projections onto the principal planes of action space. In both cases, we also show as gray pixels the distribution of main-sequence turn-off stars (MSTOs) from Myeong et al. (2018a). This is to give an idea of the range in action at any energy level occupied by the stellar halo. Both plots are color coded according to the conventional classification from Mackey & van den Bergh (2005): red circles mark the OH GCs, blue triangles the YH GCs, yellow triangles the

BD GCs, and green diamonds the Sagittarius GCs. The Sagittarius dwarf (Sgr) is also marked as a black filled square. The YH GCs all lie above a critical energy of $E_{\text{crit}} = -1.6 \times 10^5 \text{ km}^2 \text{ s}^{-2}$. The BD globulars all lie below this critical energy. We regard the identification of this critical energy E_{crit} as a reference level. Though the value of E_{crit} does depend on potential, the existence of a critical energy level is robust—it is the value of the most bound YH cluster. We argue that GCs with comparable or higher energy are all accreted from dwarf galaxies.

The BD and OH clusters form tracks in Figures 1 and 2. We can see that the BD clusters branch out toward positive J_ϕ , while maintaining low J_R and low J_z values, as befit disk orbits. They are entirely limited to $E \leq E_{\text{crit}}$. For the OH clusters, we can see a similar branching toward positive J_ϕ at low energy ($E < E_{\text{crit}}$). The low-energy OH clusters are all concentrated at low J_R . There are similarities in the morphology of the (J_R, E) distribution for the low-energy OH clusters and the the MSTOs as illustrated in Myeong et al. (2018a). In the (J_z, E) plane, the OH clusters seemingly break up into two separate branches at low energy, though it is unclear whether this is caused by dynamical or selection effects.

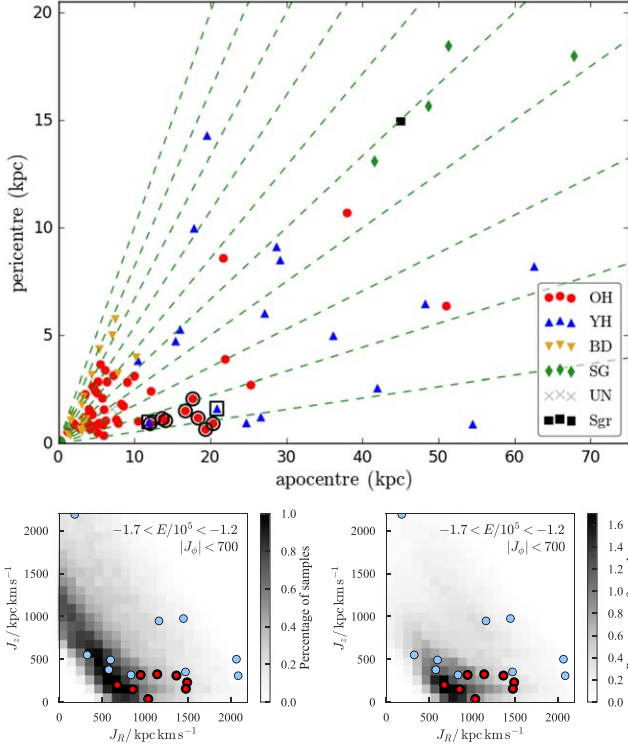


Figure 3. Upper panel: apocenters and pericenters of the GCs, color coded according to OH (red circles), YH (blue triangles), BD (yellow triangles), Sgr GCs (green diamonds), and unknown (gray cross). Sgr is also marked (black filled square). Lines of constant eccentricity from 0 to 0.9 in steps of 0.1 are shown in green. Note the Sausage GCs (black open circles as probables and open squares as possibles) all have eccentricity $\gtrsim 0.80$. Lower panels: *Gaia* selection effects. The gray pixels show the distribution of samples in action space of GCs at the observed locations of GCs, but with velocities randomly drawn from Gaussians with isotropic velocity dispersion $\sigma = 130 \text{ km s}^{-1}$ (left) and from the radially anisotropic dispersion found by Smith et al. (2009) for local halo stars (right). Only samples with $-1.7 < E/10^5 < -1.2$ and $|J_\phi| < 700 \text{ km s}^{-1} \text{ kpc}$ are shown. The actual locations of the Sausage GCs (red) and other GCs (pale blue) with $-1.7 < E/10^5 < -1.2$ and $|J_\phi| < 700 \text{ km s}^{-1} \text{ kpc}$ are superposed. In the left panel, although there is a weak bias to low J_z , it is clear that *Gaia* could have detected objects at high J_z in this energy range if they existed. In the right panel, the relative lack of high J_z GCs is expected in such a radially anisotropic DF, but the GCs at large J_R (the tips of the Sausage) are not.

There are 15 OH clusters above the critical energy ($E \gtrsim E_{\text{crit}}$). Their azimuthal action J_ϕ distribution is narrower than the low-energy ones. It resembles the tips of the “diamond-like” contours seen in the distribution of MSTOs in the metal-rich halo (Myeong et al. 2018a). Also, the radial action J_R distribution of high-energy OH clusters is extremely distended. Most of them have high radial action, tracing out a structure similar to the picture of the metal-rich halo.

Of the 15 high-energy OH clusters, there are 6 with high vertical action ($J_z \gtrsim 1000 \text{ km s}^{-1} \text{ kpc}$). They lie well apart from the main group. They have a wide spread in azimuthal (J_ϕ) and radial (J_R) actions similar to the YHs, suggesting an accretion origin. The main group are concentrated at large J_R , low J_z and low J_ϕ region in the action space, indicating radial orbits. They show surprisingly low vertical action ($J_z \lesssim 500 \text{ km s}^{-1}$)—they are actually less extended in J_z than the low-energy OH clusters and much less extended than the MSTO stars with similar energy. This tight concentration, especially in J_z , is interesting because the range of J_z becomes wider as we move to higher energy, as is demonstrated by the

Table 1

Kinematic Properties of the Eight Probable and Two Possible Sausage GCs

Name (NGC)	(v_r, v_θ, v_ϕ) (km s $^{-1}$)	e	(J_R, J_ϕ, J_z) (km s $^{-1}$ kpc)	E (km 2 s $^{-2}$)
1851	(134.8, 11.6, 28.6)	0.91	(1493, -178, 230)	-134706
1904	(46.5, -2.9, -21.5)	0.93	(1477, 51, 155)	-137390
2298	(-96.1, 41.3, -57.7)	0.79	(949, -648, 317)	-140391
2808	(-152.9, -35.5, -3.7)	0.86	(1038, 394, 35)	-152947
5286	(-202.3, 42.4, -58.3)	0.84	(856, -366, 148)	-153940
6864	(-113.0, -27.6, 24.1)	0.83	(1144, 316, 324)	-143397
6779	(159.4, 19.9, -76.9)	0.86	(677, -182, 199)	-159799
7089	(231.3, 24.1, 28.0)	0.88	(1368, -192, 309)	-139217
362	(147.1, 7.9, -33.5)	0.85	(837, -57, 317)	-159510
1261	(-113.8, 30.5, 7.2)	0.86	(1474, -393, 351)	-132973

Note. The galactic rest-frame velocity in spherical polars, the actions in cylindrical polars, the energy, and orbital eccentricity $e = (r_{\text{apo}} - r_{\text{peri}})/(r_{\text{apo}} + r_{\text{peri}})$ are all given.

MSTO sample. The eight high-energy OHs forming this main group (NGCs 1851, 1904, 2298, 2808, 5286, 6864, 6779, and 7089) are marked with black circles in Figures 1 and 2. For this group of eight, the maximum J_z is $\sim 360 \text{ km s}^{-1} \text{ kpc}$, the maximum $|J_\phi|$ is $\sim 500 \text{ km s}^{-1} \text{ kpc}$, while the minimum J_R is $\sim 700 \text{ km s}^{-1} \text{ kpc}$. In action space, their distribution is highly flattened and sausage-like. Interestingly, there are no OH clusters with comparable energy that have high vertical action J_z (see e.g., the middle panel of Figure 2). Mackey & Gilmore (2004) suggest that 15%–17% of the OH clusters might have been accreted. In our picture, at least 8 Sausage GCs (or 14 including those with very high J_z) out of 53 are accreted, in rough accord with the estimate.

The YH GCs all have $E > E_{\text{crit}}$, and show a broad spread in all actions. They include extreme prograde and retrograde members in the sample, as well as the ones with largest radial J_R and vertical J_z actions (excluding the Sgr GCs). The two black open squares in Figures 1 and 2 provide an extended selection to the Sausage GCs. They are two YH GCs (NGC 362, and NGC 1261) with a rather similar horizontal branch morphology to OH clusters (see Section 3) that also have similar actions and energy to the Sausage GCs. These are possibles rather than probables.

The upper panel of Figure 3 shows the apocenters and pericenters of the sample, with lines of constant eccentricity superposed. The *Gaia* Collaboration et al. (2018) already noted the tendency for GCs with larger apocenters to have larger eccentricities. The eight probable and two possible Sausage GCs are denoted by black open circles and open squares. They form a clump concentrated at high J_R , low J_z , and low J_ϕ , and they all have high orbital eccentricity $\gtrsim 0.80$. We can also see that most of the BD clusters have low eccentricity. There are also many OH clusters with comparably low eccentricity. The YH clusters are again widely dispersed, as they have high energy and highly spread actions.

Finally, we must consider whether selection effects could cause this. As the *Gaia* Collaboration et al. (2018) point out,

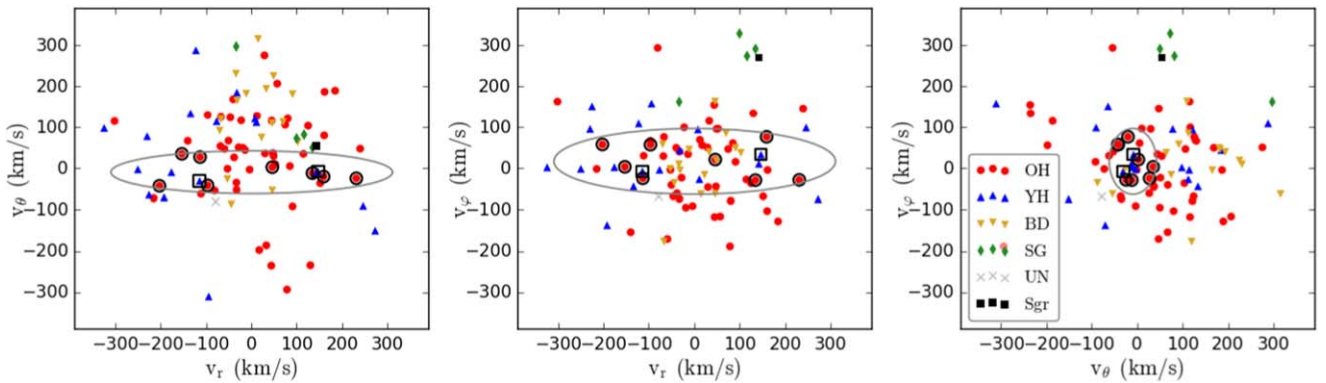


Figure 4. Velocity distribution of the GC sample, resolved with respect to spherical polar coordinates (v_r , v_θ , v_ϕ). The Sausage GCs are marked with their customary black open circles (probables) and open squares (possibles). Their extreme radial anisotropy is illustrated by the superposed ellipses with semiaxes given by the velocity dispersion in each coordinate. This plot should be compared with Figure 2 of Belokurov et al. (2018b), which shows the sausage-like velocity distributions of main-sequence turn-off stars in the SDSS-*Gaia* catalog.

GCs with high energy are more likely to be observed if they are on eccentric orbits. Even so, the middle panel of Figure 2 demonstrates that there are no OH clusters in this energy range that have high J_z . By taking the positions of GCs in our sample, and sampling their velocities from a Gaussian with $\sigma = 130 \text{ km s}^{-1}$, we show the expected distribution in action space in the lower-left panel of Figure 3. Notice that there is only a very mild bias toward low J_z , so *Gaia* should have seen any high J_z GCs at this energy range if they existed. However, if the cluster velocity distribution is highly anisotropic, as shown in the lower-right panel of Figure 3, this distribution will become more biased toward low J_z , though still the tips of the Sausage are not expected.

3. The Sausage GCs

The properties of the eight probable and two possible Sausage GCs in energy and action space are listed in Table 1.

The identification of the *Gaia* Sausage in MSTOs is most evident in velocity space. Belokurov et al. (2018b) showed that the velocity anisotropy parameter β_{MSTO} is very extreme,

$$\beta_{\text{MSTO}} = 1 - \frac{\sigma_{v_\theta}^2 + \sigma_{v_\phi}^2}{2\sigma_{v_r}^2} \approx 0.9. \quad (1)$$

Here, v_ϕ is the azimuthal velocity in the direction of the Milky Way’s rotation, v_θ is increasing toward the Milky Way’s north pole, and v_r is the radial velocity in spherical coordinates. Given that $\beta = 1$ implies that all orbits are linear straight lines through the Galactic Center, the metal-rich local halo stars are very radially anisotropic. This gives the Sausage its name, as the structure (which is also highly non-Gaussian) looks sausage-shaped in velocity space. Figure 4 shows the velocities of the GCs resolved with respect to spherical polar coordinates. The Sausage GCs have an even more extreme value of the anisotropy parameter than the Sausage MSTOs, with $\beta_{\text{GCs}} \approx 0.95$. Of course, both here and in Belokurov et al. (2018b), cuts have been used to remove stars and GCs to isolate the Sausage component.

The upper panel of Figure 5 shows age versus metallicity for the Sausage GCs, as well as seven GCs that have been claimed as associates of Sgr, specifically Terzan 7, Terzan 8, Arp 2, Pal 12, NGC 4147, NGC 6715, and Whiting 1 (Forbes & Bridges 2010). As noted by Forbes & Bridges (2010), the

age–metallicity relation for the Milky Way’s GCs reveals two distinct tracks. There is broad swathe of BD and OH GCs with a roughly constant old age of ~ 12.8 Gyr. This comprises the bulk of the sample. However, Forbes & Bridges (2010) pointed out that the Sgr GCs form a separate track that branches to younger ages, and is shown as open diamonds in Figure 5. We find that the Sausage GCs similarly follow a track that is very different from the bulk of the Milky Way’s in situ GCs. It is similar to, but vertically offset from, the Sgr track. The lower panel of Figure 5 shows the horizontal branch index versus metallicity using data from Mackey & van den Bergh (2005). The plot emphasizes the ambiguous nature of the two clusters, NGC 362 and NGC 1261. Although Mackey & van den Bergh (2005) classified them as YH clusters based on their horizontal branch morphology, they are in fact close to the dividing line. We therefore suggest that this classification can be debatable. They are kinematically close to the Sausage GCs, who may well be their true brethren.

4. Discussion

This Letter argues that there are at least 8, and possibly 10, halo GCs that belong to a single, ancient massive merger event identified by Belokurov et al. (2018b) and responsible for the *Gaia* Sausage in velocity space. The evidence is threefold. First, there is a strong prior expectation of finding a population of radially anisotropic GCs. Evidence for a major accretion event is provided by studies of the kinematics of halo MSTOs in the SDSS-*Gaia* catalog (Belokurov et al. 2018b; Myeong et al. 2018a), as well as in *Gaia* DR2 (Haywood et al. 2018). It explains the peculiar, highly non-Gaussian, radial anisotropic local velocity distribution of halo stars (hence the “*Gaia* Sausage”). The existence of the Sausage GCs supports the idea of a single event and allows us to put estimates on the mass of the progenitor. Judging from GC numbers, it must have been more massive than Fornax and comparable to the Sgr progenitor, which Gibbons et al. (2017) estimated as $5 \times 10^{10} M_\odot$ in total mass. This is in good agreement with the mass estimate provided in Belokurov et al. (2018b).

Second, just as the GCs associated with Sgr can be identified by their agglomeration in action space, so can the GCs associated with the *Gaia* Sausage. A critical energy separates the YH clusters (which have all been accreted) from the BD clusters (which are all formed in situ). The OH clusters are mainly formed in situ, though Mackey & Gilmore (2004)

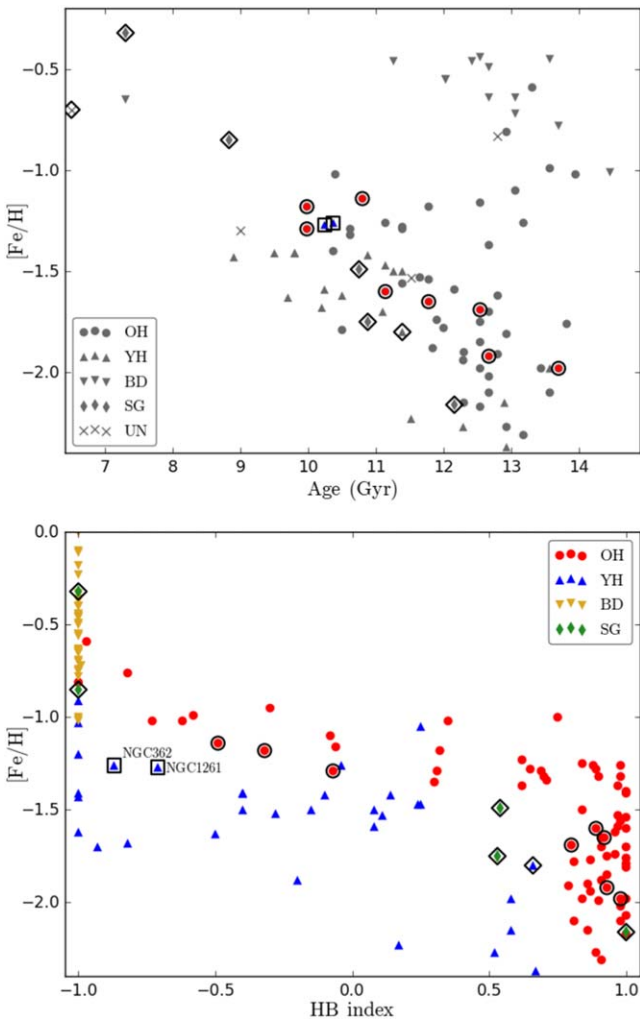


Figure 5. Upper panel: plot of the age of GCs vs. metallicity using data from Forbes & Bridges (2010). The Sausage GCs are shown with circular (probables) and square (possibles) black boundaries. Seven GCs that are claimed as former denizens of Sgr are shown as unfilled black diamonds. The sequences of Sgr GCs and Sausage GCs lie on two distinct, though closely matched, tracks. They are different from the bulk of the Milky Way GCs, which show a constant age of ~ 13 Gyr independent of metallicity. Lower panel: plot of horizontal branch morphology vs. metallicity using data from Mackey & van den Bergh (2005). The locations of the two YH clusters (NGC 362, NGC 1261) are close to the boundary and their designation is open to debate. We have included them in our extended sample of Sausage GCs, as they are kinematically similar.

suggested that 15%–17% were accreted. They straddle the critical energy. Eight of the OH clusters with $E > E_{\text{crit}}$ form a narrow, clumped, and compact distribution in action space. They have characteristic low vertical (J_z) and high radial (J_R) action. They show strong radial anisotropy ($\beta \approx 0.95$) and highly radial, eccentric orbits ($e \gtrsim 0.80$). These are exactly the characteristics expected for the Sausage GCs. There may even

be two further members—if we, for example, permit the inclusion of YH clusters.

Third, the eight GCs identified as belonging to the *Gaia* Sausage were chosen without any regard to their age or metallicity. However, these eight clusters show the typical age–metallicity trend expected from dwarf galaxies, which is additional evidence supporting their extragalactic origin. The time of infall can also be roughly reckoned from the tracks in age–metallicity space as ~ 10 Gyr or $z \sim 3$, in accord with the estimate in Belokurov et al. (2018b).

Could this peculiarity of the data be due to a selection effect, against which the *Gaia* Collaboration et al. (2018) already caution? High-energy GCs are more likely to be observed if they are on eccentric orbits. We have demonstrated that there is a weak preference for GCs in the Sausage GC energy and angular momentum range to have larger J_R than J_z . However, the Sausage GCs are a significantly more radially anisotropic population than expected purely from selection effects. This indicates that the selection effects have limited impact on our conclusions.

ORCID iDs

G. C. Myeong  <https://orcid.org/0000-0002-5629-8876>
S. E. Koposov  <https://orcid.org/0000-0003-2644-135X>

References

- Belokurov, V., Deason, A. J., Koposov, S. E., et al. 2018a, *MNRAS*, **477**, 1472
 Belokurov, V., Erkal, D., Evans, N. W., Koposov, S. E., & Deason, A. J. 2018b, arXiv:1802.03414
 Binney, J. 2012, *MNRAS*, **426**, 1324
 Binney, J., & Spergel, D. 1982, *ApJ*, **252**, 308
 Binney, J., & Tremaine, S. 2008, *Galactic Dynamics* (2nd ed.; Princeton Univ. Press: Princeton, NJ)
 Deason, A. J., Belokurov, V., & Evans, N. W. 2011, *MNRAS*, **416**, 2903
 Deason, A. J., Belokurov, V., Evans, N. W., & Johnston, K. V. 2013, *ApJ*, **763**, 113
 Forbes, D. A., & Bridges, T. 2010, *MNRAS*, **404**, 1203
 Gibbons, S. L. J., Belokurov, V., & Evans, N. W. 2017, *MNRAS*, **464**, 794
 Goldstein, H. 1980, *Classical Mechanics* (Reading, MA: Addison-Wesley)
 Harris, W. E. 1996, *AJ*, **112**, 1487, 2010 edition
 Haywood, M., Di Matteo, P., Lehnert, M., et al. 2018, arXiv:1805.02617
 Gaia Collaboration, Helmi, A., van Leeuwen, F., et al. 2018, arXiv:1804.09381
 Mackey, A. D., & Gilmore, G. F. 2004, *MNRAS*, **355**, 504
 Mackey, A. D., & van den Bergh, S. 2005, *MNRAS*, **360**, 631
 McMillan, P. J. 2017, *MNRAS*, **465**, 76
 Myeong, G. C., Evans, N. W., Belokurov, V., Sanders, J. L., & Koposov, S. E. 2018a, *ApJL*, **856**, L26
 Myeong, G. C., Evans, N. W., Belokurov, V., Sanders, J. L., & Koposov, S. E. 2018b, arXiv:1804.07050
 Posti, L., & Helmi, A. 2018, arXiv:1805.01408
 Sanders, J. L., & Binney, J. 2016, *MNRAS*, **457**, 2107
 Schönrich, R., Binney, J., & Dehnen, W. 2010, *MNRAS*, **403**, 1829
 Smith, M. C., Evans, N. W., Belokurov, V., et al. 2009, *MNRAS*, **399**, 1223
 Sohn, S. T., Watkins, L. L., Fardal, M. A., et al. 2018, arXiv:1804.01994
 Watkins, L. L., Evans, N. W., Belokurov, V., et al. 2009, *MNRAS*, **398**, 1757
 Zinn, R. 1993, in *ASP Conf. Ser.* 38, *The Globular Cluster-Galaxy Connection*, ed. G. H. Smith & J. P. Brodie (San Francisco, CA: ASP), 38